Korean J. Chem. Eng., 34(2), 566-573 (2017)
DOI: 10.1007/s11814-016-0255-7

pISSN: 0256-1115
eISSN: 1975-7220

Bubble characteristics by pressure fluctuation analysis in gas-solid bubbling fluidized beds with or without internal

Keon Bae*, Jong Hun Lim*, Joon-Hwan Kim, Dong-Ho Lee**, Joo-Hee Han**, Sung-Hee Park***, and Dong Hyun Lee*,†**

*Department of Chemical Engineering, Sungkyunkwan University, Korea
**Hanwha Chemical R&D Center, Korea
***Department of Energy Engineering, WooSuk University, Korea
(*Received 9 June 2016 • accepted 5 September 2016*)

Abstract−Bubble flow characteristics were investigated in gas-solid bubbling fluidized beds (0.3 m-I.D×2.4 m-high) with or without internals by power spectral analysis of absolute pressure fluctuation. Metallurgical grade silicon particles (MG-Si) were used as bed materials. The particle density and mean particle diameter were 2,328 kg/m^3 and 154 μm, respectively. Absolute pressure fluctuations were measured simultaneously at two different positions: plenum chamber and beds. Absolute pressure fluctuation in the beds was measured according to the axial bed height in the range of 0.1 to 0.8 m. The total sampling time of each data set was 60 s, and the sampling rate was 200 Hz. Absolute pressure fluctuation data were converted to a power spectral density (PSD) by a Fast-Fourier transform (FTT) algorithm. The PSD in the beds was separated into coherent and incoherent output power. The bubble size was estimated from the standard deviation of the spectrum of incoherent output power, which occurred due to the bubble flow. The estimated bubble size determined by incoherence component analysis was compared to various empirical correlations to determine the bubble size without internals. The estimated bubble size agreed well with the correlation by Choi et al. [19]. The internals were installed 0.45 m above the distributor. With the installation of the internals, and at the bed height of 0.5 m, the bubble diameter was decreased by 77% compared to the bubble without the internal at U_0=0.15 m/s.

Keywords: Pressure Fluctuation, Power Spectral Density (PSD), Bubble Diameter, Incoherent Component, Vertical Internal

INTRODUCTION

The contact between the gas and the particles in a bubbling fluidized bed is a very important factor for the efficiency of the reaction. The bubbles generated in the beds are used to facilitate contact between the particles, and the gas is used to induce mixing of the particles, while increasing the mass and heat transfer efficiency. On the other hand, gas bypassing that has not reacted reduces the reaction efficiency. Therefore, research on the bubble characteristics (e.g., bubble increasing velocity, bubble size) in the bubbling fluidized beds is essential. One of the methods that can be used to evenly distribute the bubbles in the beds is bubble breaking using internal fittings. The internal inhibits the growth of the bubble and redistributes the bubbles in the horizontal plane. Therefore, not only the heat and mass exchange between the gas and the particles increases, but also the eruption of the bubble is suppressed and the number of entrained particles is reduced. Dutta and Suciu [1] studied the bubble breaking phenomenon with various baffle internals in the bed of Geldart A particles (FCC). Their results demonstrated that the opening fraction from the horizontal plane of the baffle had a direct impact on the bubble splitting phenomenon. However, in the case of the Geldart B particles, if the opening ratio on the baffle is too small, the differential pressure in the beds is increased. Therefore, not only is the operating cost too high, but also bed mixing cannot be carried out smoothly. Consequently, in the pilot-scale fluidized bed reactor, a vertical internal is used to manage these disadvantages. The wetted perimeter of the internal is adjusted to induce the bubble splitting phenomenon. Observation of the change of the bubble characteristics due to the internal requires an accurate bubble measurement method. Other available methods for analyzing the characteristics of the bubbles are non-intrusive measurements (pressure fluctuation, X-ray, and Gamma-ray) and intrusive measurements (optical, capacitance probe) for measuring the voidage inside bubbles. While the measuring device using the intrusive type of method is inexpensive and the measuring instrument and handling is easy, it has a disadvantage whereby the bed voidage can only be partially measured. In addition, in the case of the dual probe, it is difficult to accurately measure the gas bubbles, as the distance between the probes is insufficient [2]. In the case of measuring using a non-intrusive type method, such as the X-ray or Gamma-ray method, the disadvantages are the difficulty in measuring using the devices at a relatively large scale and the increased expense. For these reasons, bubble size prediction has been studied extensively using pressure fluctuation analysis. A method of decoupling the pressure fluctuation of rising bubbles merely by incoherent out-put power analysis (IOP) has been stud-

†To whom correspondence should be addressed.
E-mail: dhlee@skku.edu

ied in order to correct the defect in the inaccuracy of the global pressure fluctuation analysis [3]. In comparison with measuring bubble chord lengths using the optical probe, the bubble diameter obtained from the power spectral density of the pressure time series is relatively accurate [2]. IOP analysis has been used to investigate the bubble diameter in a slurry bubble column [4] and to investigate the bubble characteristics of gas-solid bubbling fluidized beds with binary particles [5]. In the existing studies, the bubble characteristics in bubbling fluidized beds were investigated with or without screen cylindrical packing using pressure fluctuation analysis. However, in another study, the change of bubble characteristics was predicted from the main peaks of only the PSD distribution [6]. Thus, the pressure fluctuation of the bubble motion was not separated from the entire pressure fluctuation. Furthermore, the trend of the changing bubble diameter was not represented by a quantitative value.

The present study investigated the mean bubble diameter, which changes according to the equivalent diameter of the column with various internals by IOP analysis.

THEORY

Pressure fluctuation in the bubbling fluidized beds occurs for a variety of factors, such as rising gas bubbles, jetting, bubble coalescence, splitting, bubble eruption, and flow fluctuation [7]. The pressure time series is measured according to time, with a constant sampling frequency. From the measured pressure time series, the Fourier transform algorithm converts the time domain into a frequency domain. The distribution of the periods in the absolute pressure fluctuations can be analyzed from the power spectral density (PSD) in the frequency domain. Various hydrodynamic characteristics have recently been analyzed in this way; for example, the transition of fluidization regime, force balance between particles, fluctuation on the bed surface due to bubbles bursting, etc. [8-11]. In addition, the PSD distribution due to the rising gas bubbles or slug provides useful information for understanding the bubble characteristics [12-14]. Van der Schaaf et al. [3] developed a technique to estimate the average bubble diameter using the Fourier transformation of a pressure time series measured simultaneously at different column positions in a gas-solid fluidized bed. The PSD of the absolute pressure signals at the bed position can be separated into two areas related to the absolute pressure fluctuations at the plenum chamber: a coherent component (COP) and incoherent component (IOP). IOP represents the PSDs due to rising bubble or turbulence. The coherence between the two time series of bed position and plenum chamber in a fluidized bed could be used to distinguish the different components in the pressure fluctuations. The global fluctuations such as flow fluctuations, jetting, bubble coalescence, splitting, and bubble eruption, are generated throughout all the beds because their amplitudes are strong. Thus, these pressure waves are also measured in the plenum and bed position in the fluidized bed instantaneously. However, the local pressure wave due to a rising gas bubble or turbulence does not affect the pressure wave traveling through the fluidized bed. Thus, these phenomena are not measured in the plenum [3], and we can predict the coherence of the simultaneously measured waves between the bed position and plenum chamber. In the gas-solid fluidized beds, the fluctuation characteristics between bed position (x) and plenum chamber (y) are defined using the coherent function ($r^2_{xy}(f)$). The coherent function is defined as the normalization of the cross-power spectral density (cPSD) of the two time series at the bed position and plenum chamber according to each power spectral density (PSD).

$$r^2_{xy}(f)=\frac{|\phi_{xy}(f)|^2}{\phi_{xx}(f)\phi_{yy}(f)} \tag{1}$$

If the measured absolute pressure fluctuations at both the plenum chamber and bed position have the same strength response in exactly the same period, the coherent value is 1. For the case with different response and difference period, the coherent value is zero. Therefore, the PSD of the pressure time series in the bed position for the incoherent components can be distinguished from that for the coherent components by the coherent value as follows.

$$COP(f)=r^2_{xy}(f)\phi_{xx}(f) \tag{2}$$

$$IOP(f)=[1-r^2_{xy}(f)]\phi_{xx}(f) \tag{3}$$

IOP(f) is the PSD of fluctuations due to the rising bubble in the bed position. If the gas bubbles regularly pass through the measurement position with a frequency of f_b, the pressure fluctuation has a sine wave shape with an amplitude proportional to the gas diameter [15]. Therefore, the absolute pressure signal ($b_x(t)$) generated by passing the gas bubbles at the bed position (x) is expressed as a response (A_b) having a frequency of f_b.

$$b_x(t)=A_b\sin(2\pi f_b t) \tag{4}$$

$$A_b=\rho_s g(1-\varepsilon_{mf})D_b \tag{5}$$

Thus, the standard deviation of the pressure fluctuations caused by the rising gas bubble is proportional to the response of the pressure fluctuations.

$$\sigma_b=A_b/\sqrt{2} \tag{6}$$

Eq. (6) refers only to the wave of the sine function, but the form of the pressure fluctuations due to the rising bubble is more complex. The standard deviation of IOP can thus be proportional to the response ($\sigma_b \sim A_b$). Therefore, the response of the PSD of IOP can be quantified through Parseval's theorem with the standard deviation.

$$\sigma^2_{IOP}=\sum_f IOP_x(f) \tag{7}$$

By substituting Eq. (7) into Eq. (5), the standard deviation of the incoherent component could be applied according to the length scale for the prediction of bubble size.

$$\frac{\sigma_{IOP}}{\rho_s g(1-\varepsilon_{mf})}\sim D_b \tag{8}$$

As the size of the generated bubble increases, the response of IOP further increases. Therefore, the standard deviation shows similar trends to those for the bubble size. In this experiment, we predicted the bubble size by analyzing the standard deviation of the IOP with the increase of the superficial gas velocity and the meas-

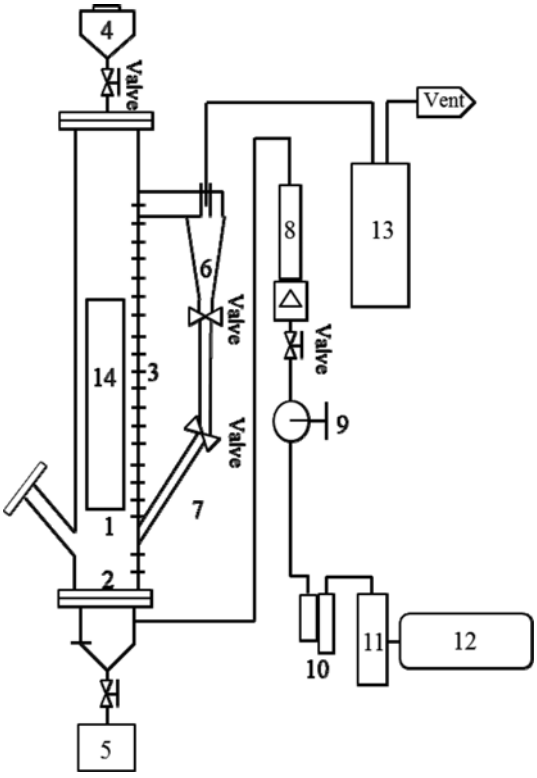

Fig. 1. Schematic diagram of experimental apparatus for bubbling fluidized bed [16].

1. Fluidized bed	6. Cyclone	11. Air dryer
2. Distributor	7. Down comer	12. Compressor
3. Pressure tab	8. Flow meter	13. Bag filter
4. Upper hopper	9. Regulator	14. Internal
5. Bottom hopper	10. Air filter	

ured bed position in the bubbling fluidized beds. Then, we evaluated the reliability of the results by comparing with the results from the existing bubble diameter equation.

EXPERIMENTAL

1. Apparatus and Particle Properties

Fig. 1 shows a schematic diagram of the bubbling fluidized beds with the column diameter of 0.3 m and the height of 2.4 m, which had been used in our previous studies [16,17]. The distributor plate was a perforated plate with an opening ratio of 0.002 with 183 holes. 40 μm mesh was placed above the holes to prevent particles leaking into the plenum chamber. Some entrained particles were recirculated through the cyclone and dipleg. The static bed height was 0.8 m and the total bed weight was 75 kg. To prevent internal absolute pressure change, after the chamber was filled with the particles, the valve connected to the chamber was closed. Metallurgical grade silicon (MG-Si) was used as a bed material, which is classified as belonging to the Geldart B group. The mean particle size was 153 μm and the particle density was 2,328 kg/m^3. The fraction of fine particles (<38 μm) was less than 2%. The material of the internals was steel and the axial length was 0.8 m. The equivalent diameter of the internal was determined by wetted perimeter of the internal, and was calculated from Eq. (9):

$$D_{eq}=\frac{4A}{L} \tag{9}$$

A is the vertical cross-section area and L is the wetted perimeter. All internals were made of stainless steel plate with a thickness of 2.0 mm. Three other internals were fabricated with equivalent diameters, D_{eq}, of 0.15, 0.17, and 0.19 m, respectively. The cross-sectional area of the internal with D_{eq}=0.15 m was 0.00105 m^2; the area of this internal has the most baffles in this study. Since the cross sectional area of internal was 1.5% or less of the sectional area of the column, it could be assumed that the internal did not significantly affect the superficial gas velocity.

Fig. 2 shows schematic diagrams of the internals used in our previous study [17]. The actual photograph of the internals is given in our previous study. Each internal was installed 0.45 m above the distributor in the beds.

2. Measurement of Absolute Pressure Signals

Fig. 3 shows the absolute pressure fluctuations measured in the bed position and plenum chamber. Absolute pressure fluctuation

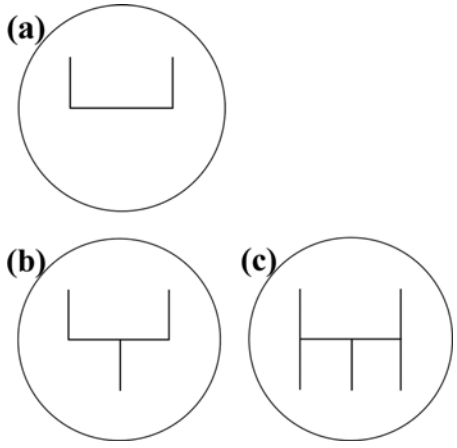

Fig. 2. Schematic diagrams of internals at various equivalent diameters: (a) 0.19 m, (b) 0.17 m, and (c) 0.15 m [17].

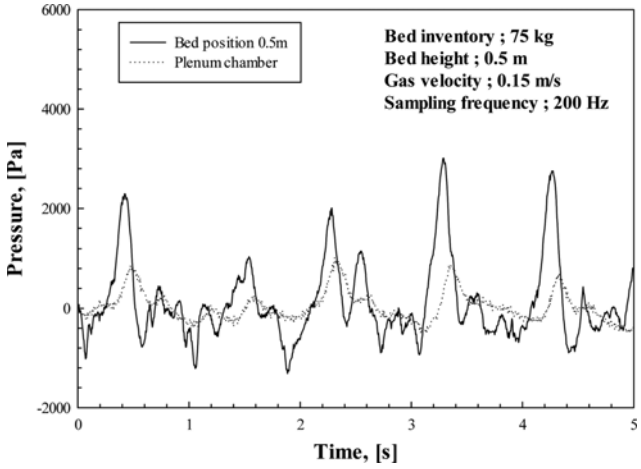

Fig. 3. Signals of absolute pressure fluctuation in an axial bed position of 0.5 m and plenum chamber.

was measured continuously at the same time in the plenum chamber and the bed. Each signal of the bed and plenum chamber was measured by an absolute pressure transducer (Setra 209 model) within a 5 psig range. 38 μm mesh was used to cover the pressure tap in order to prevent particles from flowing into the pressure transducer. The sampling frequency of the experiments varied from 100 to 1,000 Hz. The experiments confirmed the low error of 2.25%. Thus, the measurement frequency was fixed at 200 Hz for the appropriate calculation. The IOP of PSD induced by gas bubbles was measured from 0.1 to 0.8 m from the axial bed position. The superficial gas velocity ranged from 0.07 to 0.15 m/s. The internal was installed 0.45 m above the distributor. All measurements were confirmed by repeating five times.

3. Fast Fourier Transform (FFT) Algorithm

The Fast Fourier Transform (FFT) algorithm was coded using MATLAB®. The coding program converts a signal from the time domain to a representation in the frequency domain. The PSD can be used to compute the amplitude of a process by integrating the overall frequency by the FFT algorithm. We obtained the PSD at the plenum chamber and each axial bed position simultaneously from 0.1 m to 0.8 m. The PSD was calculated from an ensemble average of the five data sets.

RESULTS AND DISCUSSION

1. PSD in Bed Position and Plenum Chamber

Fig. 4 shows a comparison of the PSD measured at the bed positions of 0.1 m and 0.5 m, and at the plenum chamber. The curves were smoothed by averaging the five data sets. All PSD distributions showed a response between 0 and 10 Hz because they have a negligible value on regions higher than 10 Hz. PSDs less than 4 Hz were typically superimposed at three different measurement points. This is because the regions with a jetting/bubble formation have substantially similar intensities [2]. The peak in the range from 0.4 Hz to 1 Hz at the plenum chamber was mainly generated by jetting or flow fluctuations. To the exclusion of the region jetting/bubble formation region, the PSD distributions were measured from 0.4 Hz to 10 Hz at the bed positions of 0.1 m and 0.5 m. In this range, an additional PSD measured between 0.4 Hz and 4 Hz at the bed position was generated due to rising bubble motion. The bubble characteristics due to the differences in the measurement heights changed. These differences could be determined through the difference in the PSD distribution between the two points (bed positions at 0.1 m and 0.5 m). The measured PSD appears to lie between 2.4 Hz and 4 Hz at the bed position of 0.1 m, and predominates in the range from 0.4 Hz to 1.6 Hz at the bed position of 0.5 m. The bubbles increased in size consistently with increasing bed position due to coalescence. The measurements of the fluctuations occurring due to the coalescence of bubbles differed at the two bed positions. Because fluctuations by rising small bubbles occurred at a low bed position, a peak emerged in the high frequency region with PSD distribution. On the other hand, at a high bed position, low frequency predominated due to the rising coalesced bubbles. Consequently, by confirming that the main frequency of the PSD distribution caused by the rising bubbles occurs at any value, it is possible to compare the bubble size.

2. Standard Deviation of IOP

Fig. 5 shows the standard deviation of IOP at various gas velocities with increasing axial bed position. In all gas flow rates, the standard deviation of incoherent components due to bubble motion increased almost linearly up to the bed position of 0.5 m. The standard deviation leveled off at the bed position of 0.6 m. As discussed previously, a standard deviation of IOP is proportional to the bubble diameter. In terms of the flow characteristics of the bubble, the bubbles grew continuously due to the coalescence phenomenon. Then, if the size of the bubbles increased to two-thirds of the bed diameter, the bubbles ceased to grow further. However, this was found to be an inconsistent result when compared with the measurement result of IOP. According to the study by van der Schaaf et al. [3], the pressure caused by the rising gas bubble in the vicinity of the bed surface is determined by the particle mass present above the bubble. However, when the bubble reaches the bed surface, the absolute pressure caused by the bubble is dispersed in the bed surface direction. Thus, the standard deviation of IOP measured by the absolute pressure transducer was sharply reduced. As

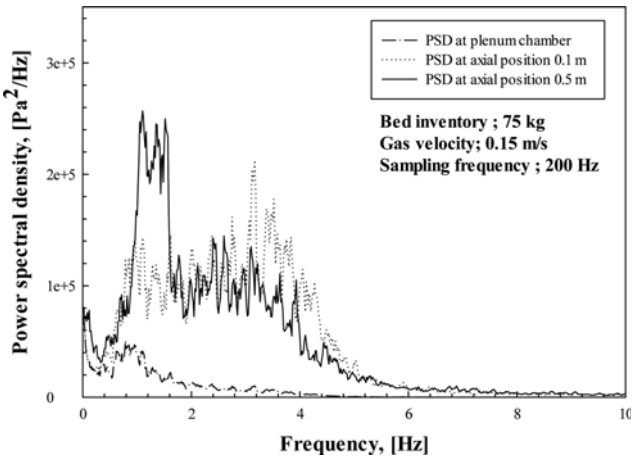

Fig. 4. Comparison of PSD of absolute pressure signals at the plenum chamber and axial bed positions of 0.1 m and 0.5 m.

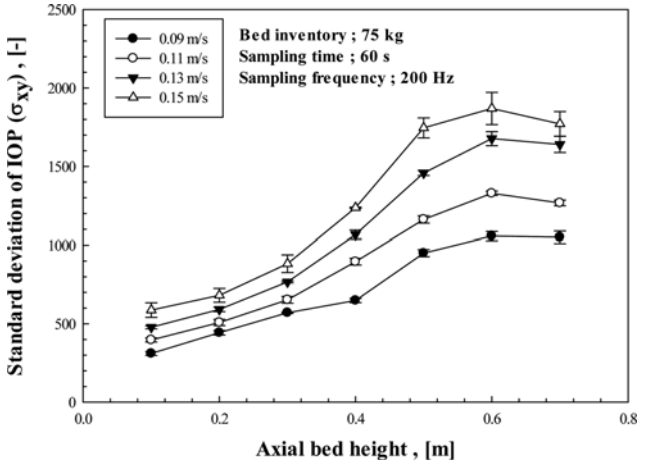

Fig. 5. Standard deviation of IOP versus axial bed height at various gas velocities.

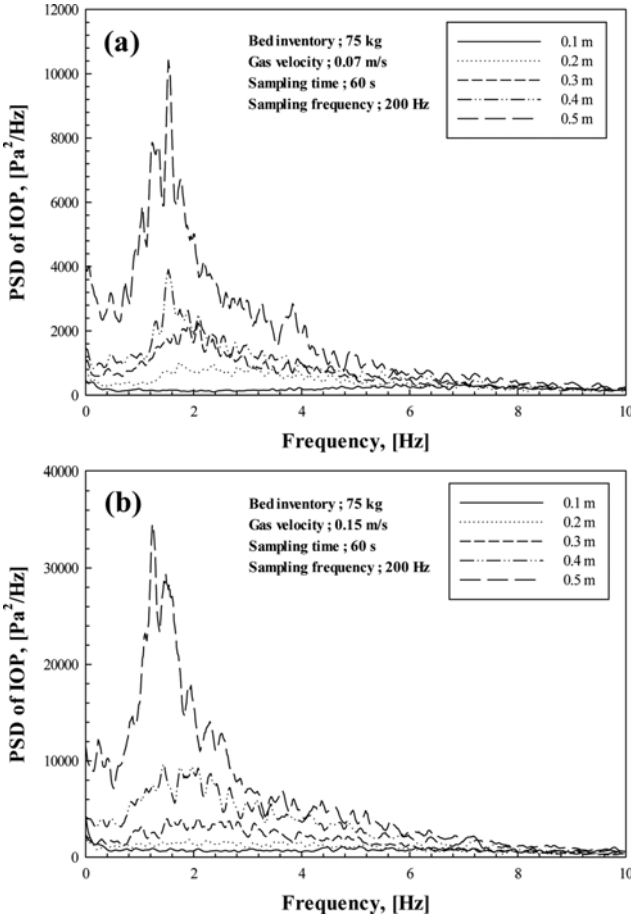

Fig. 6. Comparison of IOP of absolute pressure signals at each various axial bed position: (a) at U_0=0.07 m/s and (b) at U_0=0.15 m/s.

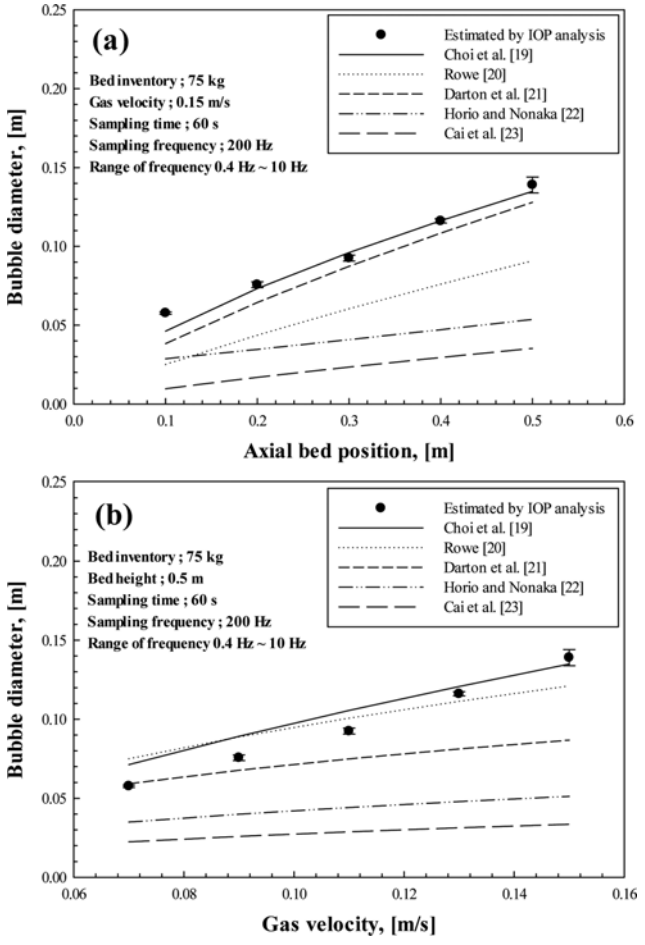

Fig. 7. Comparison between estimated bubble diameter and correlations: (a) according to axial height at U_0=0.15 m/s and (b) according to gas velocity at h=0.5 m.

a result, the response of IOP will converge to 0 because the bubble had erupted in the bed surface. Due to the limitations of such a PSD analysis, we did an analysis at the bed position up to a certain interval of 0.1 m of the increment. The maximum measurement point can be determined from the rate of increase of the IOP standard deviation. Therefore, up to the bed position of 0.5 m, we determined the maximum measurement position in the experiments and analyzed the changes of the bubble characteristic up to 0.5 m. In addition, after the internal installation the PSD was also measured at the bed position of 0.5 m.

3. Bubble Size by Incoherent Component Analysis

Fig. 6 shows the PSD distribution of IOP in various bed positions at U_0=0.07 m/s and 0.15 m/s. The response of the measured PSD distribution increased with increasing axial bed height. Also, the main peak of PSD occurred at a gradually lower frequency with increasing axial bed position. The measured bubble size increased with increasing axial bed position, and the bubble size could be predicted from the increased relative frequency of the fluctuation of a long period. These results occurred at all gas velocities. Also, when we checked the PSD measured at U_0=0.07 m/s and 0.15 m/s at the same bed position, the frequency of the main peak occurred at a lower frequency, at U_0=0.15 m/s. The bubble growth rate differed depending on the gas velocity. Regardless of the IOP distribution, the abovementioned jetting/bubble formation occurred at less than 0.4 Hz. This peak in the range below 0.4 Hz increased with increasing axial bed position, because the pressure fluctuation occurred for a long period caused by the bubble coalescence [18]. However, since the range below 0.4 Hz did not occur due to the bubble motion, the bubble diameter was estimated from the standard deviation of IOP of from 0.4 to 10 Hz.

Fig. 7 shows a comparison of the estimated bubble diameters between those obtained by IOP analysis and those from the correlations in the literature. As shown in the figure, the estimated bubble diameter increased with the increasing bed position and superficial gas velocity. Comparing the values with those obtained from the existing empirical formula, the bubble sizes calculated from the equation by Choi et al. [19] were in reasonable agreement with the bubble sizes estimated by IOP analysis. The experimental conditions and the literature bubble diameter correlations are shown in Table 1.

4. Influence of Internals

Fig. 8 shows the various PSD distributions of fluctuations by IOP analysis at various equivalent diameters. Kang et al. [7] did an analysis of the PSD of absolute pressure fluctuation depending on the mesh size of cylindrical packing in a column. However, their

Table 1. Correlations of bubble diameters in the fluidized beds

Author(s)	Correlation	Particle type	d_p (μm)	ρ_s (kg/m^3)	U_0-U_{mf} (m/s)	D (m)	Type of measurement
Choi et al. [19]	$(U_0-U_{mf})(D-D_{b0})+0.474g^{0.5}(D^{1.5}-D_{b0}^{1.5})=1.132(U_0-U_{mf})h$	Coal	340-620	2300	0.047-0.171	0.3×0.3	Electro-resistivity probe
Rowe [20]	$D_b=(U_0-U_{mf})^{1/2}(h+h_0)^{3/4}/g^{1/4}$	Ballotini, Carbon, Quartz, etc.	135-323	600-2650	0.003-0.056	0.3×0.3 0.3×0.2	X-ray photography
Darton et al. [21]	$D_b=0.54g^{-0.2}(U_0-U_{mf})^{0.4}h^{0.8}$	Ballotini, Carbon, Quartz, Glass powder, Alumina, Sand, etc.	60-323	600-2650	0.005-0.2	0.3×0.3 0.3×0.2 1, 0.61×0.61	Capacitance probe, X-ray photography
Horio and Nonaka [22]	$\left(\frac{\sqrt{D_b}-\sqrt{D_{be}}}{\sqrt{D_{b0}}-\sqrt{D_{be}}}\right)^{1-\left(\frac{\gamma M}{\eta}\right)}\left(\frac{\sqrt{D_b}-\sqrt{\delta}}{\sqrt{D_{b0}}-\sqrt{\delta}}\right)^{1+\left(\frac{\gamma M}{\eta}\right)}=\exp\left(-0.3\frac{h-h_0}{D_t}\right)$	FCC	60-450	0-48000	0.008-0.130	0.099	X-ray photography
Cai et al. [23]	$D_b=0.138h^{0.8}(U_0-U_{mf})^{0.42}\exp(-2.5\times10^{-5}(U_0-U_{mf})^2-10^{-3}(U_0-U_{mf}))$	Sand, FCC, etc.	66-700	850-3186	0-0.006	0.3×1 0.3×0.2 0.17×0.12 0.13-0.38	Absolute pressure fluctuation analysis, Probe, X-ray, etc.

research was limited to the changes in the main peak. In the present study, we decoupled the fluctuations according to the rising gas bubbles through the IOP analysis and the quantitative value, which was presented according to the standard deviation of the IOP. The fabricated internals with D_{eq}=0.15 m, 0.17 m, and 0.19 m were placed in the columns and the experimental results were compared to the experimental results without the internals. As shown in the figure, regardless of the equivalent diameter, the shape of PSD distributions was similar to the case of U_0=0.07 m/s, and the main peaks of the PSD distributions in all experiments occurred between 1.8 Hz and 1.9 Hz. Since the frequency of the main peak hardly changed according to the various equivalent diameters, the bubbles were hardly affected by the internal at U_0=0.07 m/s because the bubbles generated at U_0=0.07 m/s were relatively small. The bubble splitting phenomenon barely occurred in the presence of the internal. Thus, the reduction of bubble size due to the internal was not significant at U_0=0.07 m/s. However, the PSD distribution of IOP changed according to the various equivalent diameters with increasing gas velocity. Therefore, the estimated bubble size definitely changed and the main peak of the PSD distributions moved to a high frequency. The main peak of the PSD distribution at U_0=0.15 m/s appeared at 1.2 Hz without the internal (D_{eq}= 0.3 m). However, the main peak moved to 1.6 Hz when the internal of D_{eq}=0.15 m was installed in the column. The result showed that as the equivalent diameter of the column decreased, the frequency of pressure fluctuation decreased, as expected, due to the bubble splitting phenomenon at U_0=0.15 m/s.

Fig. 9 shows the variation of bubble diameter calculated from Eq. (8) with increasing gas velocity at various equivalent diameters. Analysis showed that the difference of bubble size according to the equivalent diameter of the internal was minimal in low gas velocity. However, without the internal, bubble coalescence was significant at U_0=0.09 m/s at the axial height of 0.5 m. In low gas velocity, bubble coalescence was significantly decreased by the internal of D_{eq}=0.19 m. However, bubble splitting rarely occurred because the bubble size was smaller than the span between the baffles. However, the bubble size increased with increasing gas velocity. Also, bubble splitting occurred frequently due to the increasing number of baffles. Therefore, the bubble size was significantly decreased with decreasing of D_{eq} at high gas velocity. The measured bubble sizes at U_0=0.07 m/s were 0.053 m in D_{eq}=0.3 m and 0.047 m in D_{eq}=0.15 m. On the other hand, the bubble sizes at U_0=0.15 m/s were 0.144 m in D_{eq}=0.3 m and 0.11 m in D_{eq}=0.15 m. The results of the experiment confirmed that the internals enabled effective bubble redistribution. While $D_{b,0.15}/D_{b,0.3}$ was reduced to 90% at U_0= 0.07 m/s, $D_{b,0.15}/D_{b,0.3}$ was reduced to 77% at U_0=0.15 m/s. Thus, because the bubbles did not sufficiently grow at the low flow rate, the bubble splitting phenomenon due to the internal was less effective. Nevertheless, since large bubbles were generated at a high flow rate, it was confirmed that the internals reduced the bubble size. The sizes of the generated bubbles differed according to the bed position and gas velocity.

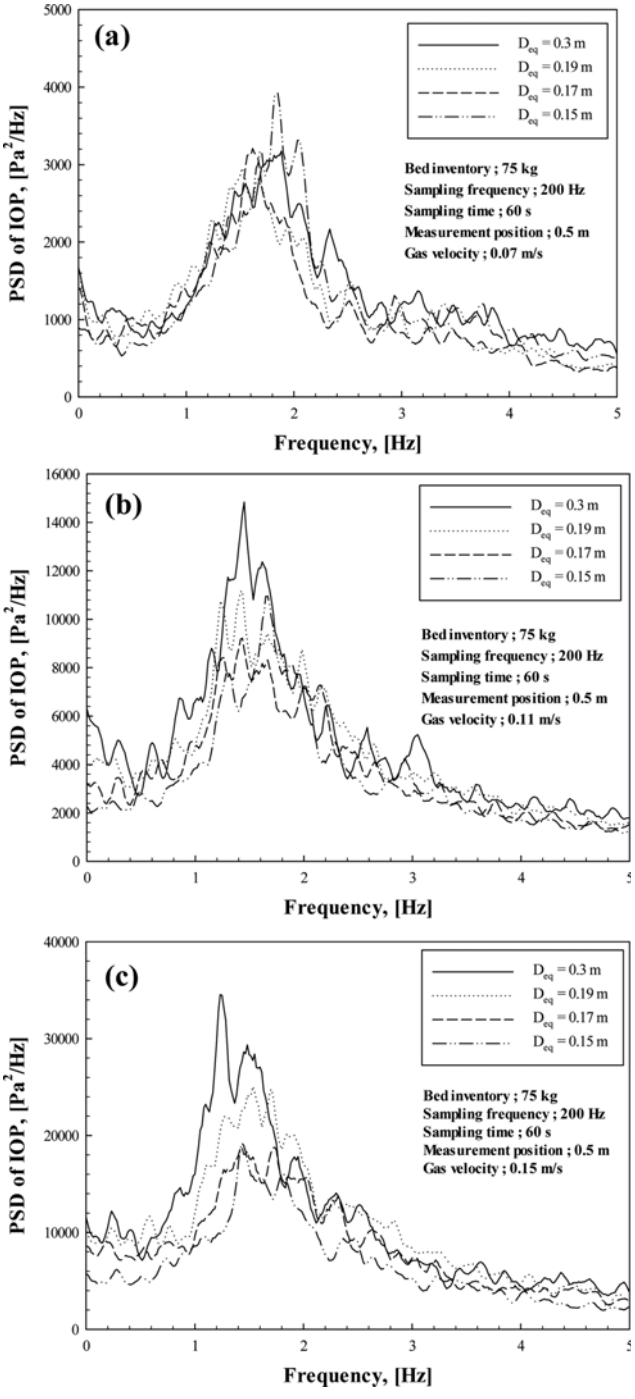

Fig. 8. Comparisons of IOP distributions in the fluidized beds at various equivalent diameters: (a) at U_0=0.07 m/s, (b) at U_0= 0.11 m/s, and (c) at U_0=0.15 m/s.

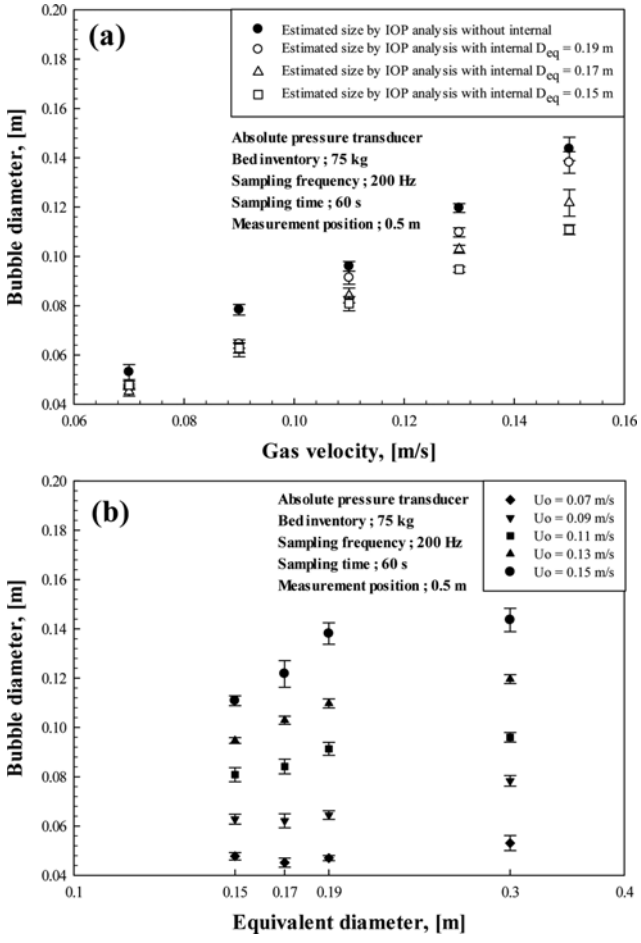

Fig. 9. Variation of the estimated bubble diameters in the gas-solid fluidized beds at various equivalent diameters: (a) According to gas velocity and (b) according to equivalent diameter.

CONCLUSION

We estimated the bubble diameter in gas-solid bubbling fluidized beds, which changes depending on the equivalent diameter of the column with various internals. The PSD of IOP due to the bubble motion was quantified for the bubble diameter through the standard deviation of IOP. The conclusions of the study are as follows.

1) The standard deviation of IOP showed a tendency to increase at the bed position of 0.5 m, and then decrease from 0.6 m upwards. The absolute pressure caused by the bubble was dispersed in the bed surface direction, while the bubble reached the bed surface. Therefore, the maximum measurement position in this experiment was determined as 0.5 m.

2) The standard deviation shows a tendency to increase with increasing gas velocity and measurement position, and the main peak of the PSD shifted to a lower frequency because the period and amplitude of fluctuations increased with increasing bubble size.

3) The estimated bubble diameter according to the standard deviation of IOP matched the correlation by Choi et al. reasonably well [19], which was carried out under experimental conditions that were most similar to those of our experiments.

4) After adjusting the D_{eq} to 0.15, 0.17, and 0.19 m with the installation of the internals, we compared the estimated bubble size with the experimental results from the general bed (D_{eq}=0.3 m). As a result, we confirmed the effective bubble redistribution due to the internals. Because bubbles do not grow sufficiently under a low gas velocity, the bubble splitting phenomenon due to the internal was less effective. However, since the large bubbles were generated at a high flow rate, it was confirmed that the internals reduced the

bubble size. While $D_{b=0.15}/D_{b=0.3}$ was reduced to 90% at U_0=0.07 m/s, it can be seen that $D_{b=0.15}/D_{b=0.3}$ was reduced to 77% at U_0= 0.15 m/s.

ACKNOWLEDGEMENTS

This study was supported by the Ministry of Knowledge Economy (MKE), the Korea Institute for Advancement of Technology (KIAT), and the Honam Institute for Regional Program Evaluation (HIRPE) through the Leading Industry Development for Economic Region. This study was also supported by the R & D Center for Valuable Recycling (Global-Top R & D Program) of the Ministry of Environment (project number of GT-14-C-01-038-0). This work was conducted under the framework of the Research and Development Program of the Korea Institute of Energy Research (KIER) (B5-2604).

NOMENCLATURE

A : cross section area of column [m^2]
A_b : average attenuation of absolute pressure wave by rising bubble [-]
$b_x(t)$: absolute pressure signal by gas bubbles at position x [-]
COP(f) : coherent output-power of pressure time series at position x [Pa^2/Hz]
D : column size [m]
D_b : bubble diameter [m]
$D_{b,0.15\,m}$: bubble diameter at equivalent diameter of 0.15 m with internal [m]
$D_{b,0.3\,m}$: bubble diameter at equivalent diameter of 0.3 m without internal [m]
D_{b0} : initial bubble diameter [m]
D_{be} : equivalent bubble diameter [m]
D_{eq} : equivalent diameter of column [m]
d_P : particle size [μm]
f_b : frequency of absolute pressure signal by ringing gas bubble [Hz]
g : acceleration of gravity [m/s^2]
h : distance from the distributor [m]
h_0 : distance from the distributor at which initial bubble forms [m]
IOP(f) : incoherent output-power of pressure time series at position x [Pa^2/Hz]
L : wetted perimeter [m]
r_{xy} : coherence function [-]
t : time [s]
U_0 : superficial gas velocity [m/s]
U_{mf} : minimum fluidization velocity [m/s]

Greek Letters

γ_M : constant correlation for bubble size in Horio and Nonaka [22] [-]
δ : constant correlation for bubble size in Horio and Nonaka [22] [-]
ε_{mf} : local voidage at minimum fluidization [-]
η : constant correlation for bubble size in Horio and Nonaka [22] [-]
ρ_s : particle density [kg/m_3]
σ_b : standard deviation of absolute pressure signal by ringing gas bubble [-]
σ_{IOP} : standard deviation of incoherent output-power [-]
$\phi_{xx}(f)$: power spectral density at x position [Pa^2/Hz]
$\phi_{yy}(f)$: power spectral density at y position [Pa^2/Hz]
$\phi_{xy}(f)$: cross-power spectral density between x and y positions [Pa^2/Hz]

REFERENCES

1. S. Dutta and G. D. Suciu, *J. Chem. Eng. Japan*, **25**, 345 (1992).
2. M. Liu, Y. Zhang, H. Bi, J. R. Grace and Y. Zhu, *Chem. Eng. Sci.*, **65**, 3485 (2010).
3. J. van der Schaaf, J. C. Schouten, F. Johnsson and C. M. van den Bleek, *Int. J. Multiphase Flow*, **28**, 865 (2002).
4. V. P. Chilekar, M. J. F. Warnier, J. van Der Schaaf, B. F. M. Kuster and J. C. Schouten, *AIChE J.*, **51**, 1924 (2005).
5. H. Chen, D. Yang and J. Cheng, *Procedia Eng.*, **102**, 799 (2015).
6. W. K. Kang, J. P. Sutherland and G. L. Osberg, *Ind. Eng. Chem. Fundamentals*, **6**, 499 (1967).
7. H. T. Bi, *Chem. Eng. Sci.*, **62**, 3473 (2007).
8. J. Verloop and P. M. Heertjes, *Chem. Eng. Sci.*, **29**, 1035 (1974).
9. O. Trnka, V. Vesely, M. Hartman and Z. Beran, *AIChE J.*, **46**, 509 (2000).
10. J. G. Sun, M. M. Chen and B. T. Chao, *Int. J. Multiphase Flow*, **20**, 315 (1994).
11. J. Li and J. A. M. Kuipers, *Chem. Eng. Sci.*, **58**, 711 (2003).
12. J. F. Davidson, *Trans. Inst. Chem. Eng.*, **39**, 230 (1961).
13. P. W. K. Kehoe and J. F. Davidson, *AIChE Symp. Ser.*, **69**, 34 (1973).
14. J. Baeyens and D. Geldart, *Chem. Eng. Sci.*, **29**, 255 (1974).
15. P. S. B. Stewart, *Trans. Inst. Chem. Eng.*, **46**, 60 (1968).
16. J. H. Lim, Y. Lee, J. H. Shin, K. Bae, J. H. Han and D. H. Lee, *Powder Technol.*, **266**, 312 (2014).
17. J. H. Lim, J. H. Shin, K. Bae, J. H. Kim, D. H. Lee, J. H. Han and D. H. Lee, *Korean J. Chem. Eng.*, **32**, 1938 (2015).
18. J. van der Schaaf, J. C. Schouten and C. M. van den Bleek, *Powder Technol.*, **95**, 220 (1998).
19. J. H. Choi, J. E. Son and S. D. Kim, *Ind. Eng. Chem. Res.*, **37**, 2559 (1998).
20. P. N. Rowe, *Chem. Eng. Sci.*, **31**, 285 (1976).
21. R. C. Darton, *Chem. Eng. Res. Des.*, **55**, 274 (1977).
22. M. Horio and A. Nonaka, *AIChE J.*, **33**, 1865 (1987).
23. P. Cai, M. Schiavetti, G. De Michele, G. C. Grazzini and M. Miccio, *Powder Technol.*, **80**, 99 (1994).